Nucleation of fullerenes as a model for examining the formation of soot

Seung Hyun Chung and Angela Violi[a)]
Department of Mechanical Engineering, University of Michigan, Ann Arbor, Michigan 48109-2125, USA

(Received 10 January 2009; accepted 9 February 2010; published online 5 May 2010)

The formation of soot begins with the nucleation of nanoparticles, a process difficult to model due to the complexity of the constituent particles. Fullerenes have characteristics resembling the particles found in soot, but their simpler structure makes simulations more tractable. We propose that the nucleation of fullerenes may serve as a window to the formation of soot nuclei. Using molecular dynamics simulations, we analyze the nucleation rates of homomolecular systems of C_{60}, C_{80}, C_{180}, and C_{240} fullerenes as function of temperature and molecular mass. For temperatures lower than 1000 K, the four systems show similar characteristics, with significant nucleation rates, due to the low energy that favors binding. At higher temperatures, the high kinetic energy limits the binding probability between fullerenes, and molecular clusters are only detected in systems composed of C_{180} and C_{240}. The analysis shows that particles with molecular masses between those of C_{80} and C_{180} could be critical for the transition from monomers to clusters. The computational findings are then related to experimental data of combustion-generated particles present in the literature to assess the feasibility of a physical nucleation pathway in high temperature regimes. The results obtained using molecular dynamics simulations highlight the importance of a physical nucleation pathway to describe the formation of molecular clusters when the particle concentration exceeds a critical value. These results represent the first step toward a more complete description of nanoparticle formation and soot nucleation in high temperature regimes. © *2010 American Institute of Physics*. [doi:10.1063/1.3345630]

I. INTRODUCTION

Nucleation is a widely used term across many fields of science and technology with examples ranging from vapor condensation to protein crystallization. Most of these apparently different phenomena share common threads requiring the overcoming of an energetic barrier and the formation of an initial nucleus.[1] These characteristics apply also to the process of soot nucleation, which bridges the transition from gaseous hydrocarbons to macromolecular building blocks (nanoparticles) that eventually turn into soot. In combustion conditions, however, the high temperatures and large pools of radicals make the process of nanoparticle formation and growth very complex, and chemical reactions together with physical nucleation paths play important roles. As a consequence, along with the difficulties to study the process experimentally due to its time and length scales, particle nucleation still remains the least understood step within the soot formation process.[2,3]

Polycyclic aromatic hydrocarbons (PAHs) have often been invoked as important compounds for the soot nucleation process.[4,5] One of the first papers published on this topic was by Stein and Fahr,[6] who studied the stability of benzenoid polyaromatic molecules as function of temperature and acetylene and hydrogen concentrations.

Various research groups analyzed the intermolecular binding of this class of compounds;[3,7–9] Miller[8] calculated the lifetimes of PAH dimers in flame conditions and concluded that agglomeration becomes important only for collisions of PAH whose mass exceeds ~800 amu, since they can form dimers with lifetimes longer than the characteristic time for chemical growth and, therefore, contribute to particle growth. Schuetz and Franklach[9] investigated the collision of two pyrene molecules using semiempirical molecular dynamics (MD) methods and showed that aromatic dimers of species as small as pyrene can survive long enough to evolve into soot nuclei; approximately 15% of the collisions at 1600 K resulted in dimers, with the majority lasting 2–8 ps and a substantial fraction lasting longer (~17 ps). A similar study on lifetimes of aromatic molecules linked by aliphatic chains (AALH) and pericondensed aromatics (PCAH) (Ref. 10) has shown an increase in the dimer lifetime with an increase in molecular mass. Recently, Herdman and Miller[3] published a detailed study of the intermolecular potentials for PAH clusters showing that the total binding energy increases with each additional layer of PAH and approaches an asymptotic limit that depends on the molecular size. Additional work, however, is required to address the importance of PAH agglomeration in combustion conditions and, mostly important, to link the lifetime of dimers with their further growth to form soot nuclei.

During the past several years, our group studied the formation of carbonaceous nanoparticles as result of chemical reactions between small hydrocarbons,[11–14] using a combination of MD and kinetic Monte Carlo (kMC) methodologies. The kMC explores the conformational space defined by the interactions between gas-phase species and nanoparticles,

[a)]Author to whom correspondence should be addressed. Electronic mail: avioli@umich.edu.

 © 2010 American Institute of Physics

Downloaded 11 May 2010 to 141.212.136.141. Redistribution subject to AIP license or copyright; see http://jcp.aip.org/jcp/copyright.jsp

while the MD module relaxes the nanoparticle structures at flame temperatures. This novel methodology, embedded in the atomistic model for particle inception (AMPI) code, describes the transition from gas-phase species to incipient particles via chemical interactions and it keeps track of chemical as well physical properties, such as particle composition, morphology, surface area, volume, etc.[12,15] The AMPI method has been very successful in reproducing some flame characteristics, and recently it has been employed by our group to study the formation of nanoparticles in counterflow diffusion flames of propane,[13] to assess the importance of chemical growth mechanisms in different conditions. In this last study, we identified combustion regimes where the formation of nanoparticles via chemical reactions was not enough to justify the experimental data on particle concentrations. We, therefore, concluded that an additional mechanism, based on physical interactions of PAH/PAH and nanoparticle/PAH, needed to be considered to describe the transition from small hydrocarbons to nanoparticles.

Following up on these results, in this study, we explore the dependence of molecular sizes and concentrations on the physical nucleation of nanoparticles in a wide range of temperatures. To this end, MD simulations are used to study systems composed of carbonaceous nanoparticles (fullerenes C_{60}, C_{80}, C_{180}, and C_{240}) in the temperature range 500–2000 K. There are two main reasons for choosing fullerenes as representatives for nanoparticles: (i) Fullerenes have a graphene-like shell structure resembling the aromatic part of nanoparticles,[3,7–9,13] and (ii) fullerenes of various sizes have similar morphologies with minimal steric hindrance, and it is, therefore, easy to single out the effect of particle size on coagulation rate. After presenting the methodology and the computational results in terms of nucleation behavior as function of particle size and temperature, Sec. III B reports a discussion of the computational results for fullerene nucleation in the context of soot formation and available experimental data.

The MD results obtained in this study show the feasibility of a physical nucleation process to describe the growth of nanoparticles in specific combustion conditions. These new findings complement our previous study on chemical growth of nanoparticles[11] and show that the nucleation process can be the result of physical and chemical pathways, whose relative importance is dictated by combustion conditions.

II. METHODOLOGY

A. Model

Homomolecular systems of C_{60}, C_{80}, C_{180}, and C_{240} were simulated using the canonical *NVT* ensemble with cubical periodic boundary conditions. The familiar form of a short-range 6–12 Lennard-Jones (LJ) potential was employed to model the non-bonded interactions between atoms. The total conformational energy between two fullerene molecules was defined as

$$V = \sum_{ij} -\frac{A}{r_{ij}^{6}} + \frac{B}{r_{ij}^{12}}, \tag{1}$$

where A and B are the attractive and repulsive constants and r_{ij} is the distance between two interacting atoms. The values of A and B were taken from the discrete carbon-carbon potential for C_{60}–C_{60} developed by Girifalco *et al.*[16,17] ($A=15.2$ eV Å^6 and $B=34.8\times10^3$ eV Å^{12}), who computed the potential parameters by matching the calculated values of the cohesive energy and lattice constant to experimental data.[16] This potential has been used by other research groups to compute molecular properties of C_{60} and compared with experimental data for the heat of sublimation and lattice constant.[16,18] The discrete atom-atom model was used in this study to facilitate the scale up of the potential to bigger fullerene molecules. The LJ potential cutoff was set at 30 Å and the molecules were considered to be rigid. The elimination of intramolecular potential is consistent with the continuum model proposed by Girifalco,[16] which simplifies the system by averaging the potential over the surfaces of the molecules. This model has been used to study the growth of fullerene clusters, interaction of C_{60} with a graphite surface and thermal expansion of C_{60}.[19] The temperature was controlled using the Nosé–Hoover thermostat. Keeping the temperature constant is very important since an inefficient thermalization may have a strong influence on the results. A recent work by Wedekind *et al.*[20] investigated the influence of carrier gases and thermostats on nucleation processes described with MD. The authors analyzed the efficiency of velocity rescaling, Nosé–Hoover, and a carrier gas (mimicking the experimental condition), and reported that the choice of the thermostating method does not have a significant influence on the nucleation rate, obtaining deviations of less than a factor of 1.7. The trajectories were integrated using the velocity Verlet method, using a time step of 0.05 ps. All calculations were performed using the DL_POLY _2.18 software package.[21]

B. Initial conditions

The concentration of particles was set at 8×10^{18} cm^{-3}, with 343 molecules for the C_{60} and C_{80} systems ($35\times35\times35$ nm^3 box) and 125 molecules for the C_{180} and C_{240} cases ($25\times25\times25$ nm^3 box). The value of particle concentrations chosen for the simulations is higher than the experimental values reported in the literatures. To address this point, however, in Sec. III B we report a detailed discussion of the effect of particle concentration on the degree of clustering of nanoparticles. The systems of molecules were initially simulated at high temperatures (~3500 K) to sample three initial configurations. The temperature range analyzed spans of 500–2000 K considering intervals of 100 K for a total of 16 temperatures.

C. Identification of clusters

An important component of this study is the definition of molecular clusters. While the simplest way is to use the distance cutoff, this criterion can become increasingly inadequate in a scenario where small clusters are constantly pro-

Downloaded 11 May 2010 to 141.212.136.141. Redistribution subject to AIP license or copyright; see http://jcp.aip.org/jcp/copyright.jsp

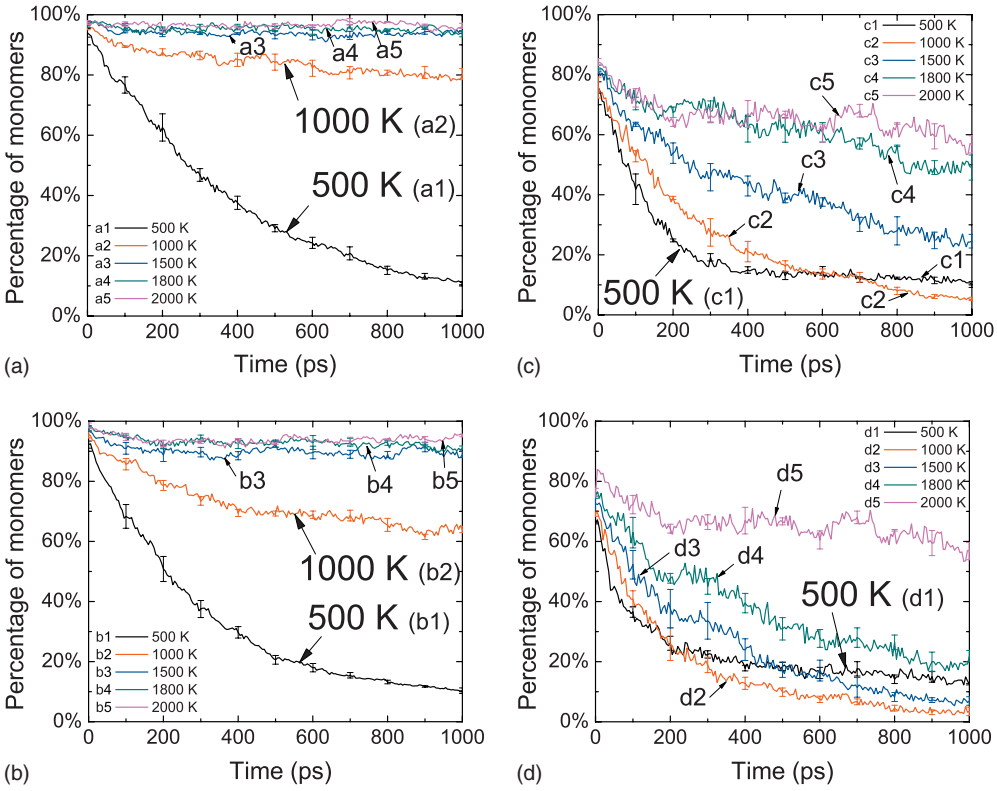


FIG. 1. Percentages of C_{60}, C_{80}, C_{180}, and C_{240} fullerene molecules in the state of monomers as function of time at various temperatures.

duced and destroyed, since the distance cutoff will overestimate the number of clusters by not distinguishing between mere collisions and agglomeration events. Therefore, in addition to this first criterion, we also compared the rotational and vibrational energies of a molecular pair to the binding potential energy, defined as the sum of atomistic intermolecular interactions. This criterion can be expressed as follows:

$$\frac{\Sigma m_i}{2}\left(\frac{\Sigma v_i m_i}{\Sigma m_i} - \frac{\Sigma v_i m_i + \Sigma v_j m_j}{\Sigma m_i + \Sigma m_j}\right)^2 + \frac{\Sigma m_j}{2}\left(\frac{\Sigma v_j m_j}{\Sigma m_j} - \frac{\Sigma v_i m_i + \Sigma v_j m_j}{\Sigma m_i + \Sigma m_j}\right)^2 < \sum_i \sum_j \left[\left(-\frac{A}{r_{ij}^{12}}\right) + \left(\frac{B}{r_{ij}^{6}}\right)\right], \quad (2)$$

where i and j are the atoms in two different molecules and A and B are the LJ parameters used in the MD simulations. Under the assumption that both molecules are internally rigid, the left side represents the sum of the rotational and vibrational energies of a newly formed dimer. These energies are associated with the reaction coordinate of dissociation of the dimer and therefore inequality (2) can be a strong indicator of the stability of dimers. For a system composed of N molecules, $N(N-1)$ molecular pairs were evaluated.

However, since other degrees of freedom than the ones reported in Eq. (2) can lead to the dissociation of the cluster, this method has an inherent inaccuracy. For example, even if a dimer has low vibrational and rotational energies, a high translational energy can lead to the instant dissociation of the molecular pairs via a collision event. At the same time, it is also difficult to clearly define molecular dimers during a simulation because their lifetimes and stabilities vary greatly. Therefore, we visually inspected the computed trajectories at various time steps and compared the behavior of the molecules with the results obtained using the criteria discussed above. The agreement in terms of important quantities (e.g., the size of biggest cluster, the number of clusters, and the number of monomers) was very good.

III. RESULTS AND DISCUSSIONS

A. Simulation results

Figures 1 and 2 report the percentages of fullerenes present in the system as monomers and the number of fullerenes per cluster for C_{60}, C_{80}, C_{180}, and C_{240} molecules as function of time at different temperatures. At 500 K, the systems show a significant number of "sticky" collisions and the percentage of monomers decreases by 80% over a time interval of 1000 ps reaching an average of 3.5 to 4 fullerenes per cluster. The nucleation rate at 500 K, identified by the disappearance of monomers in the system, is the highest among the conditions investigated. However, for the systems composed of C_{180} and C_{240}, the growth of nuclei at 500 K reaches a plateau between 600 and 700 ps. This result can be explained using the Maxwell–Boltzmann molecular speed distributions of two homogeneous systems at different temperatures, as their conceptual plots are drawn in Fig. 3(a). At T_{low} (e.g., 500 K in our simulations), molecules with relatively high translational energies participate to the formation of nuclei since they are able to reach each other within a relative short time, and their energy levels favor binding

Downloaded 11 May 2010 to 141.212.136.141. Redistribution subject to AIP license or copyright; see http://jcp.aip.org/jcp/copyright.jsp

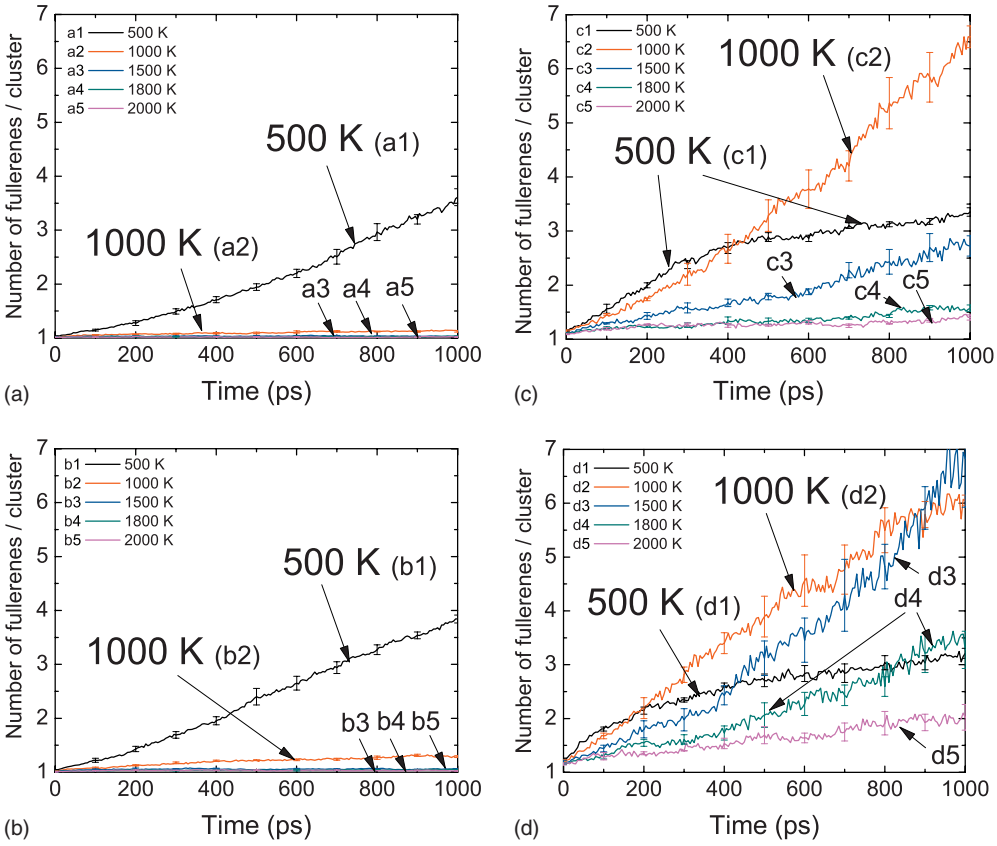


FIG. 2. Mean cluster size (number of fullerenes per cluster) as a function of time at various temperatures.

[Fig. 3(b)]. Since this process can be faster than the energy transfer, molecules with low translational kinetic energies require longer time to reach the adjacent species and remain in the system as monomers. In this situation, shown as T_{low} in Fig. 3(c), the system looks "frozen" due to the low speed of the molecules and nuclei. At higher temperatures, this effect is negligible since the binding probability is relatively low due to the high kinetic energies of the molecules. These two scenarios can explain the crossover behaviors reported in Fig. 2 for curves c1 and c2 [Fig. 2(c)] and curves d1, d2, and d3 [Fig. 2(d)].

At 1000 K, the four systems (C_{60}, C_{80}, C_{180}, and C_{240}) show different behaviors. The average size of C_{60} and C_{80} clusters does not exceed 1.35 fullerenes (curves a2 and b2 in Fig. 2) and the percentages of monomers in the systems are ~80% for C_{60} and ~60% for C_{80} at the end of 1 ns simulation. C_{60} and C_{80} nuclei are constantly formed but they dissociate because of thermal fluctuations and the majority of the clusters exist as dimers. Differently, in these conditions, C_{180} and C_{240} systems still show nucleation events. At 2000 K, only the biggest molecules—C_{240}—present some nucleation events.

To further investigate the behavior of the systems, we computed the Lindemann index (LI),[22] that is an indicator of the molecular disorder. While the LI is typically used to identify phase transitions by observing an increase above a critical value or a departure from linearity in a global LI set,[23] in this study, the LI is used to investigate the nucleation process. The formation of a nucleus lowers the LI significantly and a departure from linearity in a global set can be interpreted as the onset of nucleation process. The LI is defined as

$$\delta_{lin} = \frac{2}{N(N-1)} \sum_{i,j(i<j)=1}^{N} \frac{\sqrt{\langle R_{ij}^2 \rangle - \langle R_{ij} \rangle^2}}{\langle R_{ij} \rangle}, \tag{3}$$

where R_{ij} is the distance between the centers of masses of the molecules, and the angle brackets indicate a time averaged quantity. In equilibrium conditions, the LI does not depend on the sampling period if the values are averaged for long time. However, in this study, the LI changes over time due to the nonequilibrium conditions. Therefore, in order to compare the results obtained for the four systems at different temperatures, we averaged the values of LI between 0.75 and 1 ns with 5 ps intervals and the results are reported in Fig. 4.

The system composed of C_{60} molecules shows the highest values of LI over the temperature range 500–1000 K, implying that the molecules are in a thermally disordered state and the formation of nuclei is not significant. At low temperatures, the values of the LI decrease and the system shows a more ordered state with the formation of nuclei. The system composed of C_{80} molecules has an overall value of the LI slightly lower than the one obtained for the C_{60} ensemble. Large fullerenes (C_{180} and C_{240}) present significantly lower values of the LI over the entire temperature range 500–2000 K when compared with the C_{60} and C_{80} systems, especially between 800 and 1500 K. The observed behaviors suggest that the mass of the molecules is an important factor for the nucleation behavior at flame temperatures and a mass

Downloaded 11 May 2010 to 141.212.136.141. Redistribution subject to AIP license or copyright; see http://jcp.aip.org/jcp/copyright.jsp

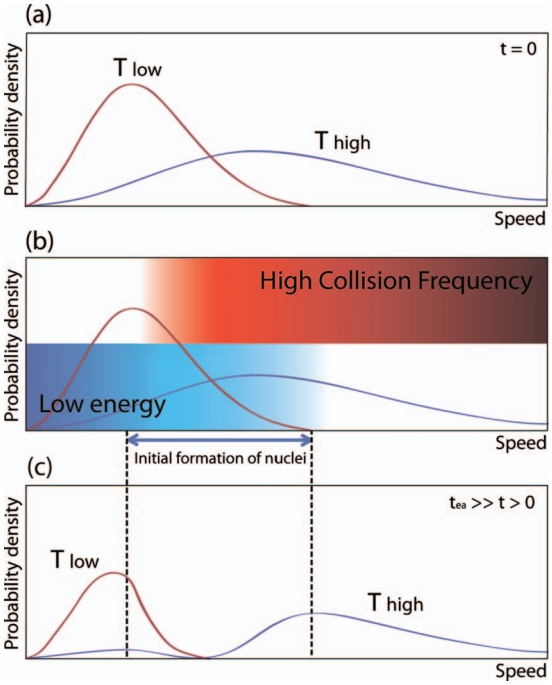


FIG. 3. Speed probability density functions of molecules at two temperatures using the Maxwell–Boltzmann distribution. Both (a) and (b) are at $t=0$ and (c) is at t immediately after few collisions between molecules. These conceptual graphs are drawn using an arbitrary scale.

value between those of C_{80} and C_{180} could represent a critical value for the transition from monomers to clusters.

Figure 5 reports the intermolecular potential curves for C_{60}, C_{80}, C_{180}, and C_{240} obtained from the interatomic LJ potential. The attractive wells become narrower and deeper as the masses of the molecules increase due to the presence of more electrons in the systems and stronger London forces. This result agrees qualitatively with the findings of Herdman and Miller.[3] At any given temperature, while the masses of the molecules contribute to the nucleation by reducing the molecular speed and hence decreasing the collision rate, the effect of deeper interaction potentials overcomes the effect of low collision rate due to the increased sticking probability.

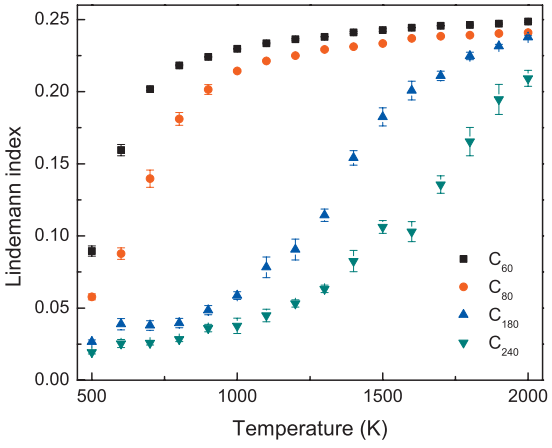


FIG. 4. LI for the systems composed of C_{60}, C_{80}, C_{180}, and C_{240} fullerene molecules. The values are averaged over 0.25 ns time window with 5 ps sampling intervals. Temperature ranges from 500 to 2000 K with increments of 100 K.

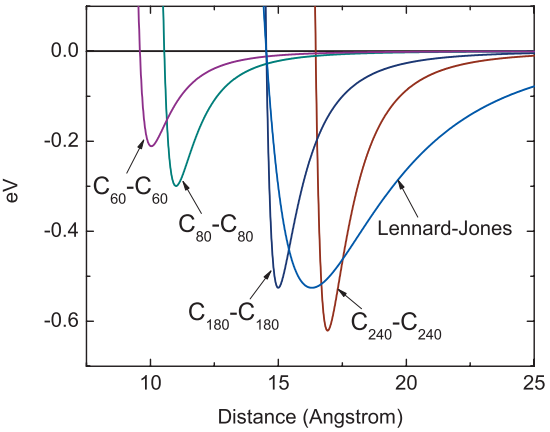


FIG. 5. Calculated potentials for C_{60}, C_{80}, C_{180}, and C_{240} systems obtained from the interatomic LJ potential between carbon atoms. The LJ potential fitted to C_{180} fullerene's ϵ (depth of the potential well) and σ (distance at which the interparticle potential is zero) is reported for comparison.

B. Implications for soot nucleation

The goal of this study is to relate the results obtained using MD simulations to the nucleation process occurring in flame environments, characterized by the presence of gaseous species along with nanoparticles. In a previous work reported by our group,[13] we analyzed two different configurations of counterflow diffusion flames to determine the effect of combustion environments on particle formation. The first configuration was a soot-formation-oxidation (SFO) propane flame with the flame front located on the fuel side and the gas velocity directed toward the flame. The second one was a soot-formation (SF) propane flame with the gas velocity directed toward the stagnation plane and particles moving away from the flame front, which was located on the oxidizer side. The two flame conditions showed different mechanisms for the formation of particle agglomerates, and hence two interesting scenarios for the development of a model to describe the growth of nanoparticles.

For these systems, using the AMPI method,[13,14] we concluded that the growth rate of nanoparticles based on chemical interactions between gas phase species and particles was important in SFO flames, showing very good agreement with experimental data, but the conditions depicted in SF configurations required additional growth mechanisms. In Fig. 6 we report the experimental data of soot volume fraction, particle diameter, and number density obtained by Kang *et al.*[24] for the SF configuration. Although the experiments illustrates the formation of particles between 5 and 7.7 mm, the chemical growth described via the AMPI method shows the formation of nanoparticles only between 7 and 7.7 mm (gray area in Fig. 6). This result is mainly due to the low temperature, which limits the importance of a chemical growth process.

Outside the gray area (Fig. 6), the soot volume fraction increases by one order of magnitude from z=7 mm to z~5 mm, corresponding to the stagnation plane. Since particle coagulation and agglomeration do not change the soot volume fraction, and at the same time a growth mechanism based on chemical kinetics is ruled out due to the low temperature conditions, a nucleation mechanism based on physi-

Downloaded 11 May 2010 to 141.212.136.141. Redistribution subject to AIP license or copyright; see http://jcp.aip.org/jcp/copyright.jsp

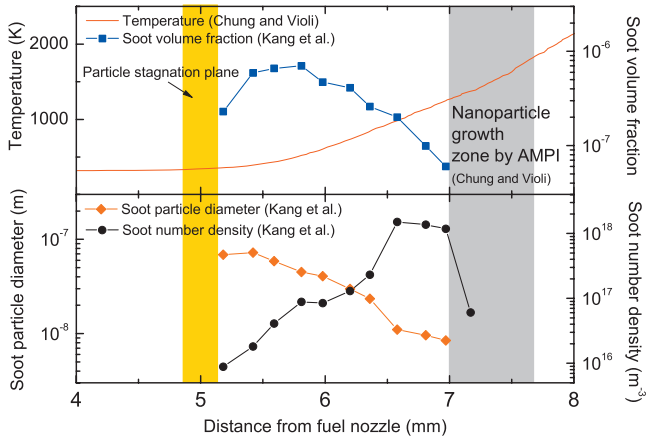


FIG. 6. Experimental soot volume fraction, soot particle diameter, and soot number density in counter-flow diffusion flame of propane [Adapted from Kang *et al.* (Ref. 24)]. Computed temperature profile from Chung and Violi (Ref. 13). The grey area (Nanoparticle growth zone by AMPI) depicts the region where the chemical nucleation is significant according to Chung and Violi (Ref. 13). Total distance between the fuel and the oxidizer nozzles is 14.2 mm and the profiles from 4 to 8 mm are plotted in this graph.

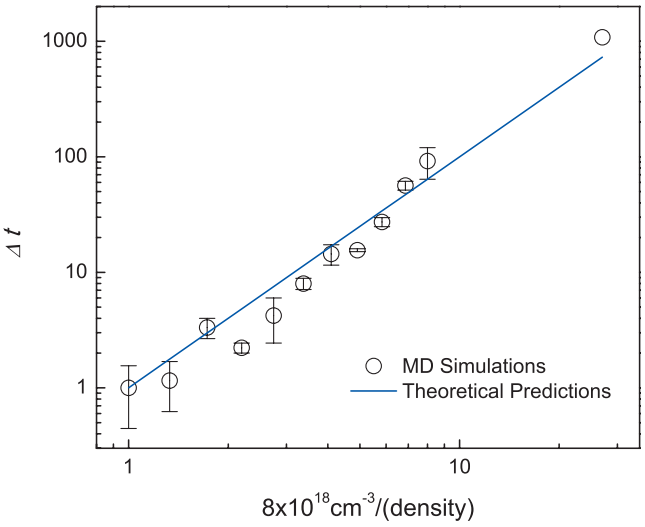


FIG. 7. Comparison between MD simulation results and the prediction by Eq. (6). The circles display MD simulation time when the percentage of monomer molecules decreases below 75% and the line indicates the theoretical prediction.

cal interactions between nanoparticles could explain the experimental evidences, especially in the range of z=6.5–7.0 mm.

In order to determine the feasibility of this hypothesis, below we relate the results obtained in the previous sections using MD simulations to flame conditions. In a gas phase environment, there is a random distribution of collisions between molecules, so that the occurrence of a collision does not affect the likelihood of a subsequent collision.[25] Therefore, it is reasonable to assume that the description of nanoparticle formation in flames can be performed without explicitly including gaseous species. In this case, the number of collisions over a given period of time can be preserved and it can be assumed that the nucleation time in a relatively dense system determined using MD simulations, can be associated with the time in a flame. The collision frequency of molecule A can be expressed as

$$Z = n_A^2 \pi (b_{\text{coll}})^2 \bar{v}_A, \tag{4}$$

where n_A and $\bar{v}_A$ are the concentration and average velocity of molecules A in the system, respectively, and b_{coll} is the collision diameter. To simplify the problem, we assume that the number of collisions between particles is linearly dependent on the nucleation time. This assumption is justified by the fact that, at a certain temperature, molecular energies will have similar distributions even for different density systems and, therefore, the percentage of effective collisions that can lead to cluster formation does not depend on system density. Thus, we can relate the nucleation time scale of the MD simulation to the nucleation process in flames,

$$Z_{\text{MD}}/Z_{\text{Flame}} = \Delta t_{\text{Flame}}/\Delta t_{\text{MD}}, \tag{5}$$

where Δt_{MD} is the nucleation time scale obtained from MD simulations and Δt_{Flame} is the experimental time in a flame. The collision diameters b_{coll} for the molecules analyzed with MD and the ones in the flame environment are the same in this case. Similarly, if the temperatures of the MD simulations and flame conditions are identical, the average velocities of the particles $\bar{v}_A$ are equivalent. Combining Eqs. (4) and (5), we obtain

$$\Delta t_{\text{Flame}} \cong \Delta t_{\text{MD}} \times n_{\text{MD}}^2/n_{\text{Flame}}^2. \tag{6}$$

This expression correlates Δt_{Flame} with the MD simulations time and particle concentrations.

In order to validate this correlation, additional MD simulations were carried out varying the density of the system. Twelve different densities were sampled and, for each case, the simulation times when the percentage of monomers decreases below 75% were sampled and compared with theoretical values obtained using Eq. (6). Figure 7 reports the relationship between density and Δt, showing very good agreement between the values obtained using MD simulation and prediction obtained with Eq. (6). Therefore, the correlation described in Eq. (6) can be justified for this analysis.

To assess the relative importance of a chemical mechanism versus a physical process for the formation of clusters, we define $t_{1.5}$ as the simulation time when the average size of a cluster reaches 1.5 fullerenes. For T>1000 K, the cluster sizes of the systems composed of C_{60} and C_{80} do not reach 1.5 over the MD simulation time, as reported in Fig. 8. Differently, for the C_{180} and C_{240} systems, $t_{1.5}$ is of the order of 10^1 or 10^2 ps for the entire temperature range considered. However, as reported in Fig. 6, the temperature of the gray area exceeds 1300 K and, in these conditions, the time scale for the chemical growth calculated using the AMPI code was between 0.1 and 1 ms.[13] For T>1300 K MD simulations predict $t_{1.5}$ of the order of 10^2 ps, even for systems composed of C_{240}. The most important difference between the conditions analyzed by MD simulations and flame conditions is the difference in particle density. Using Eq. (6), if Δt_{MD} is 10^2 ps and the system density is $n_{\text{MD}}=8\times10^{18}$ cm^{-3}, the Δt_{Flame} is 10 ms when $n_{\text{Flame}}=8\times10^{14}$ cm^{-3} or Δt_{Flame} is 0.1 ms if $n_{\text{Flame}}=8\times10^{15}$ cm^{-3}. Both cases, however, are not practical to describe nanoparticle growth in these flame conditions. In the first scenario, 10 ms is too slow to represent a

Downloaded 11 May 2010 to 141.212.136.141. Redistribution subject to AIP license or copyright; see http://jcp.aip.org/jcp/copyright.jsp

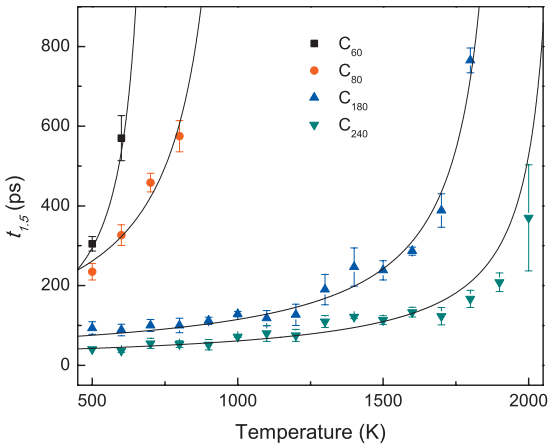


FIG. 8. Values of $t_{1.5}$, defined as the simulation time for the mean size of the clusters to reach 1.5 fullerenes for the C_{60}, C_{80}, C_{180}, and C_{240} systems of fullerenes.

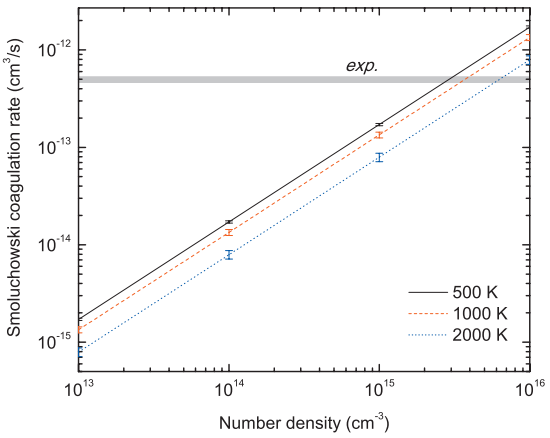


FIG. 9. Smoluchowski coagulation rates for the system composed of C_{240} as a function of number density at different temperatures.

viable growth mechanism when compared with the chemical growth rate calculated by the AMPI method, which is two orders of magnitude lower.[13] In the second case, the number density of $n_{\text{Flame}}=8\times10^{15}$ cm^{-3} is unrealistically high, when considering the maximum carbon atom number density that can be supplied by a fuel. Therefore, as reported by Chung and Violi,[13] a chemical mechanism for the cluster growth is expected to be the dominant pathway for the soot nucleation process in this region.

This conclusion changes when particles move out of the gray area toward the stagnation plane. The temperature in this region ranges from 400 to 1300 K (Fig. 6) and $t_{1.5}$ of C_{240} is of the order of 10^1 ps. If $t_{1.5}$ is used in Eq. (6), we obtain a $O(\Delta t)=1$ ms when the density of $n_{\text{Flame}}=8\times10^{14}$ cm^{-3}, which is comparable with the time scale for chemical growth in the gray region. While a density value of 8×10^{14} cm^{-3} can be considered very high in view of the current experimental predictions,[26] it can still be realistic. To show this, we simplify the problem by calculating the total carbon atom density of propane. If the mole fraction of the fuel in a system is 0.5, which is the case for the SF flame shown in Fig. 6, the available carbon number density at T=1000 K and P=1 atm is 1.1×10^{19} cm^{-3}. Since the carbon atom number density of C_{240} is 1.9×10^{17} cm^{-3}, if its molecular density is $n_{\text{Flame}}=8\times10^{14}$ cm^{-3}, then only 1.7% of the entire carbon atom content contributes to the formation of C_{240}. This value is realistic. Santoro *et al.*[27] reported that in some conditions the percentage of fuel carbon converted to soot particles can reach 10%–15% in sooting zones under atmospheric pressure and Flower and Bowman[28] demonstrated that at high pressure (~10 atm) over 50% of the fuel carbon can be converted to soot particles. Therefore, a density value of 8×10^{14} cm^{-3} may be achieved for nanoparticles in flames, because their sizes are much smaller than soot particles.

When this last result is combined with the previous AMPI analysis, we can conclude that the nucleation process can be active over the entire soot zone, from the high temperature oxidation side to the low temperature stagnation plane, and flame conditions determine the relative importance of a purely chemical growth mechanism, a physical-clustering process or their combination. These results can also explain the experimental increase in the soot volume fraction in the low temperature region starting from ca. z=7 mm toward the stagnation plane.

A second set of experimental studies reporting data on nanoparticle size distributions and population is represented by *in situ* methods, such as UV-visible light scattering, fluorescence, and extinction measurements.[26,29] When the wavelength of the light λ is much larger than the size of particles, the absorption and scattering can be expressed as

$$K_{\text{obs}}=-\frac{6\pi}{\lambda}\text{Im}\left\{\frac{\tilde{m}^2-1}{\tilde{m}^2+2}\right\}f_v, \tag{7}$$

$$Q_{vv}=\frac{3\pi^3}{2\lambda^4}\left|\frac{\tilde{m}^2-1}{\tilde{m}^2+2}\right|^2 f_v d^3, \tag{8}$$

where $\tilde{m}$ is a complex index of refraction, f_v is the volume fraction, and d is the mean diameter. As the measured light scattering is the sum of scattering due to the gas-phase products of combustion as well as of the high molecular mass structures and soot particles, the excess scattering due to gas-phase compounds was estimated and subtracted from the experimental scattering values. For a premixed fuel rich laminar flame with a C/O ratio of 0.51, which is below the sooting threshold, Minutolo *et al.*[26] reported the average size and the number density of the particles as ca. 2.3 nm and 8×10^{12} cm^{-3}, respectively. For a C/O ratio of 0.77, which corresponds to sooting environments, the number density of particles was around 7×10^{13} cm^{-3} when the average size of the particles was ca. 2.5 nm. In these conditions, the experimental Smoluchowski coagulation rate

$$k=-\frac{1}{N^2}\frac{dN}{dt}, \tag{9}$$

where N is the number concentration, is $k\approx5\times10^{-13}$ cm^3/s.[26] To analyze these experiments, we determined the Smoluchowski coagulation rate from MD simulations of a system composed of C_{240} that has mass and size similar to the nanoparticles experimentally identified by Minutolo *et al.*[26] Figure 9 shows the Smoluschowski coagulation rate versus the number density at different tempera-

Downloaded 11 May 2010 to 141.212.136.141. Redistribution subject to AIP license or copyright; see http://jcp.aip.org/jcp/copyright.jsp

tures obtained from MD simulations. The Smoluchowski coagulation rate is linearly related to the number density because the MD time scale is quadratically dependent on the number density of the MD simulation. For the experimental number density of 7×10^{13} cm^{-3}, the Smoluchowski coagulation rates are 1.2×10^{-14}, 9.4×10^{-15}, and 5.5×10^{-15} cm^3/s for T=500, 1000, and 1500 K, respectively. These values are one order of magnitude lower than the experimental rate of 5×10^{-13} cm^3/s. In our simulations, the experimental value of 5×10^{-13} cm^3/s can be reached only if the number density is of the order of 10^{15} cm^{-3}. Interestingly, this value is very similar to the one proposed for the SF flame.

From these analyses, we can infer that, at least for some flame conditions, the number density of nanoparticles should be of the order of 10^{15} cm^{-3} to explain the nucleation process. As mentioned above, however, the value of density proposed in this study is quite high when compared with currently available experimental data. One possible explanation could be the uniqueness of the refractive index $\tilde{m}$ assigned to all the nanoparticles in the flame environment, since this value is a critical factor in determining results from UV optical diagnostics. Future work is necessary to address this point.

IV. CONCLUSIONS

In this paper we investigated the nucleation process of carbonaceous nanoparticles in the temperature range 500–2000 K using MD simulations with the overall goal to determine the importance of a physical nucleation process in different flame conditions. Four systems, composed of C_{60}, C_{80}, C_{180}, and C_{240} fullerenes, were considered and the simulations were carried out over the temperature range 500–2000 K.

For temperatures lower than 1000 K, the four systems show similar behaviors in terms of clustering. At higher temperatures, however, molecular clusters are formed only with molecular sizes of C_{180} and C_{240}.

When the computational results are related to flame conditions, nucleation of small particles, such C_{60} and C_{80}, cannot justify the experimental values of nanoparticles growth, except for temperatures lower than 1000 K. On the other side, systems composed of bigger nanoparticles (C_{180} and C_{240}) showed considerable clustering between 500 and 2000 K during the first 1 ns of simulation time.

The results obtained using the LI, an indicator of the molecular disorder, show that large fullerenes (C_{180} and C_{240}) present significantly lower values of the LI when compared with the C_{60} and C_{80} systems, especially between 800 and 1500 K and this suggests that a mass value between of the ones of C_{80} and C_{180} can be critical for the nucleation behavior at flame temperatures.

The MD results obtained in this study help complement our previous study on chemical growth of particles using the AMPI model in counter diffusion flame[13,14] by adding feasibility to an alternative route—a nucleation process—in the low temperature region. The computational results were also correlated with the experimental data from UV-visible light scattering and absorption experiments.[26,29] The analysis reveals that the number density of nanoparticles in a sooting flame could be ca. 10^{15} cm^{-3} for particle sizes as large as C_{240} to undergo a significant physical nucleation process. While this value of particle density is high compared with available experimental results, the percentage of fuel carbon conversion to soot particles is indeed reasonable, thus showing the feasibility of this assumption. The results reported in this paper demonstrate that the physical nucleation pathway plays a role in particle nucleation if the density of particles and their sizes are above critical values. Therefore, particle nucleation is the result of physical and chemical pathways, and the combustion conditions determine the relative importance of these two routes.

ACKNOWLEDGMENTS

This research was funded by the National Science Foundation Grant No. CTS 0553764 and by the Department of Energy, Office of Basic Energy Sciences, Division of Chemical Sciences, Geosciences, and Biosciences under Contract No. DE-SC0002619. High performance computations were supported in part by the National Science Foundation through TeraGrid resources (Grant. No. TG-CHE080066N.

[1] J. Wedekind, D. Reguera, and R. Strey, J. Chem. Phys. **125**, 214505 (2006).
[2] M. Frenklach, Phys. Chem. Chem. Phys. **4**, 2028 (2002); J. Appel, H. Bockhorn, and M. Frenklach, Combust. Flame **121**, 122 (2000).
[3] J. D. Herdman and J. H. Miller, J. Phys. Chem. A **112**, 6249 (2008).
[4] M. J. Castaldi, N. M. Marinov, C. F. Melius, J. Huang, S. M. Senkan, W. J. Pit, and C. K. Westbrook, Sym. (Int.) Combust., [Proc.] **26**, 693 (1996); M. Frenklach, D. W. Clary, J. W. C. Gardiner, and S. E. Stein, *ibid.* **20**, 887 (1985); B. D. Crittend and R. Long, Combust. Flame **20**, 359 (1973); C. S. McEnally and L. D. Pfefferle, Combust. Flame **115**, 81 (1998).
[5] M. Frenklach and H. Wang, Sym. (Int.) Combust., [Proc.] **23**, 1559 (1991).
[6] S. E. Stein and A. Fahr, J. Phys. Chem. **89**, 3714 (1985).
[7] J. H. Miller, K. C. Smyth, and W. G. Mallard, Sym. (Int.) Combust., [Proc.] **20**, 1139 (1985).
[8] J. H. Miller, Sym. (Int.) Combust., [Proc.] **23**, 91 (1991).
[9] C. A. Schuetz and M. Frenklach, Proc. Combust. Inst. **29**, 2307 (2002).
[10] D. Wong, R. Whitesides, C. A. Schuetz, and M. Frenklach, in *Combustion Generated Fine Carbonaceous Particles*, edited by H. Bockhorn, A. D'Anna, A. F. Sarofim, and H. Wang (Karlsruhe University Press, Villa Orlandi, Anacapri, 2007), p. 245.
[11] A. Violi, G. A. Voth, and A. F. Sarofim, *30th International Symposium on Combustion* (Combustion Inst., Chicago, 2004), Vol. 30, p. 1343; A. Violi, A. F. Sarofim, and G. A. Voth, *3rd Mediterranean Combustion Symposium* (Taylor & Francis, Marrakech, Morocco, 2003), Vol. 176, p. 991; A. Violi and A. Venkatnathan, J. Chem. Phys. **125**, 054302 (2006); A. Violi, Combust. Flame **139**, 279 (2004); A. Violi and G. A. Voth, in *1st International on High Performance Computing and Communications (HPCC 2005)*, edited by L. T. Yang, O. F. Rana, B. DiMartino, and J. Dongarra (Springer, Berlin, Sorrento, Italy, 2005), Vol. 3726, p. 938; A. Violi, A. F. Sarofim, and G. A. Voth, Combust. Sci. Technol. **176**, 991 (2004).
[12] A. Violi and S. Izvekov, Proc. Combust. Inst. **31**, 529 (2007).
[13] S. H. Chung and A. Violi, Carbon **45**, 2400 (2007).
[14] S. H. Chung and A. Violi, in *Combustion Generated Fine Carbonaceous Particles*, edited by H. Bockhorn, A. D'Anna, A. F. Sarafim, and H. Wang (Karlsruhe University Press, Villa Orlandi, Anacapri, 2007), p. 321.
[15] S. L. Fiedler, S. Izvekov, and A. Violi, Carbon **45**, 1786 (2007); S. Izvekov, A. Violi, and G. A. Voth, J. Phys. Chem. B **109**, 17019 (2005); S. Izvekov and A. Violi, J. Chem. Theory Comput. **2**, 504 (2006).
[16] L. A. Girifalco, J. Phys. Chem. **96**, 858 (1992).
[17] L. A. Girifalco, M. Hodak, and R. S. Lee, Phys. Rev. B **62**, 13104 (2000).

Downloaded 11 May 2010 to 141.212.136.141. Redistribution subject to AIP license or copyright; see http://jcp.aip.org/jcp/copyright.jsp

[18] C. S. Yannoni, R. D. Johnson, G. Meijer, D. S. Bethune, and J. R. Salem, J. Phys. Chem. **95**, 9 (1991).
[19] J. P. K. Doye and D. J. Wales, Chem. Phys. Lett. **247**, 339 (1995); C. Rey, J. García-Rodeja, L. J. Gallego, and J. A. Alonso, Phys. Rev. B **55**, 7190 (1997).
[20] J. Wedekind, D. Reguera, and R. Strey, J. Chem. Phys. **127**, 064501 (2007).
[21] W. Smith and T. R. Forester, J. Mol. Graph. **14**, 136 (1996).
[22] F. A. Lindemann, Phys. Z. **11**, 609 (1910).
[23] L. J. Gallego, J. Garcia-Rodeja, M. M. G. Alemany, and C. Rey, Phys. Rev. Lett. **83**, 5258 (1999); A. Piatek, A. Dawid, and Z. Gburski, J. Phys.: Condens. Matter **18**, 8471 (2006).
[24] K. T. Kang, J. Y. Hwang, S. H. Chung, and W. Lee, Combust. Flame **109**, 266 (1997).
[25] I. J. Steinfeld, S. J. Francisco, and L. W. Hase, *Chemical Kinetics and Dynamics* (Prentice Hall, New York, 1989).
[26] P. Minutolo, G. Gambi, A. D'Alessio, and S. Carlucci, Atmos. Environ. **33**, 2725 (1999).
[27] R. J. Santoro, T. T. Yeh, J. J. Horvath, and H. G. Semerjian, Combust. Sci. Technol. **53**, 89 (1987).
[28] W. L. Flower and C. T. Bowman, Sym. (Int.) Combust., [Proc.] **21**, 1115 (1988); **20**, 1035 (1985).
[29] P. Minutolo, G. Gambi, and A. D'Alessio, Sym. (Int.) Combust. [Proc.] **27**, 1461, 1998.

Downloaded 11 May 2010 to 141.212.136.141. Redistribution subject to AIP license or copyright; see http://jcp.aip.org/jcp/copyright.jsp